energies

MDPI

Article

Planning Evening Net-Load Ramp Adequacy for High Distributed-PV Penetration in a Receiving-End City: A Coverage-Margin Approach

Yanna Gao [1,†], Hong Dong [1], Fanhong Zeng [1], Junwei Li [2,†] and Hui Liao [2,*]

[1] Power Grid Planning Research Center, Guangzhou Power Supply Bureau, Guangzhou 510640, China; 13512778095@163.com (Y.G.); 13922108817@163.com (H.D.); 1206868572@qq.com (F.Z.)
[2] Guangzhou Institute of Energy Conversion, Chinese Academy of Sciences, Guangzhou 510640, China; lijw1@ms.giec.ac.cn
* Correspondence: liaohui@ms.giec.ac.cn
† These authors contributed equally to this work.

Abstract

Photovoltaic (PV) expansion concentrates balancing pressure in the evening hours of receiving-end cities, and flexibility planning needs a benchmark that connects extreme ramping demand with deliverable resource capability. Existing adequacy practice compares installed capacity with peak load, so the evening operating window remains unpriced when installed capacity appears sufficient. Here we establish an evening net-load-ramp coverage-margin model, whose coverage margin equals deliverable resource capability, spanning power output, sustained energy, and interday replenishment, minus the annual 99th-percentile daily evening net-load ramp. In City A, the annual extreme evening ramp rose from 2610 MW in 2023 to 4328 MW in 2025, with the 2025 resource portfolio already at the coverage boundary (−116 MW under the historical-response capability convention), and specified 2030 scenarios span a 3338 MW interval between resource-lag shortfall and coordinated-development surplus. A held-out check confirms the cross-year stability of this state within the City A dataset. Portfolios with equal single-day power margins diverge over consecutive high-ramp days, because storage duration and interday replenishment determine whether coverage persists. These findings shift flexibility planning from static capacity matching toward coordinated configuration of power, deliverable energy per window, storage duration, and recoverable energy, and external validation in other receiving-end cities follows local recalibration.

Keywords: distributed photovoltaics; receiving-end city; evening net-load ramp; flexibility adequacy; energy-constrained resources; scenario planning

Check for updates

Academic Editor: Sanath Alahakoon, Md Ohirul Qays

Received: 14 September 2026
Revised: 26 October 2026
Accepted: 9 November 2026
Published: 27 November 2026

Copyright: © 2026 by the authors. Licensee MDPI, Basel, Switzerland. This article is an open access article distributed under the terms and conditions of the Creative Commons Attribution (CC BY) license.

1. Introduction

China's rapid photovoltaic (PV) expansion is reshaping the planning conditions of receiving-end urban power systems [1]. In City A, distributed PV reduces midday net load while concentrating operating pressure in the evening restoration period. Planning for receiving-end systems requires coordinated local flexible resources, interregional support, and storage inventories over the daily operating cycle [2–4]. When a credible tail-ramp criterion is absent, installed capacity can appear sufficient while the evening operating window remains exposed. Net-load-ramp adequacy, therefore, requires a joint assessment of power, energy, and duration.

Dispatch in the provincial grid that serves City A combines technical security rules with market clearing. Provincial spot markets, piloted first in Guangdong, clear day-ahead and real-time energy through security-constrained unit commitment and economic dispatch [5]; interprovincial transfers follow medium- and long-term schedules set before the operating day [4]; and pumped-storage plants recover capacity costs through a two-part tariff and operate under system-operator instructions [6]. Evening restoration in City A is, therefore, delivered by locally dispatched gas- and coal-fired units, pumped storage, and interprovincial import whose schedules respect both security constraints and market outcomes. The present study evaluates the physical deliverability that both layers share.

Flexible-capacity expansion requires matching capacity with resource response and replenishable energy. Under rising high-PV penetration, insufficient planning accumulates two sources of risk: response–capacity mismatch and energy depletion over consecutive days. In 2025, the 99th percentile of City A's daily evening net-load ramp reached 4328 MW, while the corresponding coverage margin was −116 MW. Consecutive high-ramp days can consume storage energy faster than it can be replenished. During 19–21 March 2025, pumped-storage state of charge (SOC) declined from 100% to 78.4%, 56.9%, and 35.3%, and the 3 h equivalent cumulative residual energy approached 1.29×10^4 MWh. These risks require a planning framework that combines response calibration, scenario adequacy, and intertemporal energy states under one daily tail-ramp criterion.

Prior research provides the foundations for this task. Supply-side studies use duck-curve and probabilistic-ramp analyses to characterize high-quantile operating conditions under rising PV penetration [7–10], and recent work extends this line to data-driven modeling of PV-driven residual load [11] and to net-load forecasting for high-renewable-penetration grids [12]. Evaluation studies construct flexibility-adequacy models that organize the power, energy, and ramping dimensions of resource portfolios [7,13], with recent applications to transmission-side flexibility under CVaR-constrained operation [14] and to capacity-adequacy mechanisms that remunerate flexibility [15], while ramping-product and dispatch studies describe the operational mobilization of flexible resources [16–18]. Studies of pumped-hydro storage, battery storage, and long-duration storage represent intertemporal energy constraints through storage state and recharge dynamics [19–25]; recent adequacy analyses quantify the capacity contribution of PV with embedded battery storage [26], cross-regional peak-shaving schedules coordinate pumped storage with wind and PV [27], and receiving-end planning studies co-optimize flexibility resources across renewable bases and HVDC-connected load centers [28]. These studies establish methods for probabilistic characterization of evening ramps, flexibility assessment, resource dispatch, and storage-state analysis. Planning for high-distributed-PV receiving-end cities nevertheless retains three gaps. First, power, energy, and duration commonly enter adequacy assessment separately; a common coverage margin has yet to compare the coverage states produced by resource-development scenarios and the single-day power-closure equivalence of alternative portfolios. Second, the tail percentile of the daily evening net-load ramp and its sampling confidence interval rarely enter city-level resource planning; a common probabilistic benchmark is needed for the growth of annual extreme evening ramps, the 2025 resource boundary, and 2030 coverage states. Third, single-day evening stress captures power closure within one operating window, whereas storage SOC, resource duration, and interday replenishment have yet to enter a sustained-delivery assessment of resource pathways during consecutive high-ramp days.

This study asks whether City A's evening flexible-resource development stays ahead of the growing evening-ramp demand, and which resource constraint binds first when development lags. Three nested questions structure the analysis. The first question quantifies the planning demand and the present boundary: to what level have PV expansion and

load-profile change raised City A's annual extreme evening net-load ramp, and where does the 2025 resource portfolio stand relative to the resulting coverage boundary? The second question evaluates how specified 2030 combinations of PV development and resource commissioning transform this demand into distinct coverage states. The third question follows one closure pathway into sustained operation, examining how resource duration and interday replenishment shape the deliverable trajectory during consecutive high-ramp days. To answer these questions, the study integrates state-dependent resource-response curves, scenario-based evening-ramp tail projections, stationary block bootstrap inference, and an SOC state model in a unified power–energy–duration framework. The framework supports consistent, planning-relevant comparisons of flexible-resource scale, portfolio composition, and sustained operating conditions in City A and other receiving-end cities after local recalibration of PV visibility, interprovincial import availability, resource response, and replenishment conditions.

2. Data and Methods

2.1. Study System, Data Sources, and Temporal Alignment

The analysis covers City A over 2023–2025. Generation-side observations at 5 min resolution include coal-fired generation, gas-fired generation, photovoltaic (PV) generation, hydropower, biomass generation, and storage generation. Hourly dispatch records include centrally dispatched load, interprovincial import (the power City A receives under interprovincial transactions, positive for import), pumped-storage operation, and network losses. Hourly meteorological observations enter the calibration and derating context as covariates.

Annual peak loads were 22,040 MW in 2023, 23,997 MW in 2024, and 23,944 MW in 2025. Unless otherwise noted, normalized planning quantities use the 2025 peak load $P_{\text{peak}} = 23{,}944$ MW; the pooled descriptive response bins of Section S3 in the Supplementary Materials are normalized by each year's corresponding peak load. Missing-source and pre-commissioning observations were excluded. The 2025 daily-shape analysis excluded 51 of 365 calendar days, comprising 33 weekend days and 18 weekdays; the remaining 314 valid daily shapes define the annual extreme-ramp sample and retain a documented non-uniform selection pattern. The complete data categories, audit rules, and sample pipeline are provided in Section S1 of the Supplementary Materials.

Hourly dispatch snapshots were mapped to 5 min clock boundaries for the daily ramp component and the resource-response curves. The native 5 min absolute PV-ramp series retained its original resolution for the fast-scale tail calculation. Energy quantities throughout the resource assessment represent AC-side deliverable energy.

2.2. Net Load and Ramp Definitions

The dispatched-load series L_t denotes gross system load including network losses, and distributed PV is metered separately as the generation-side series $P_{\text{PV},t}$ (Section S1 of the Supplementary Materials). Net load N_t was defined as dispatched load less PV generation:

$$N_t = L_t - P_{\text{PV},t}. \tag{1}$$

Section S1 of the Supplementary Materials gives the field definitions and the system power balance.

The daily evening net-load ramp of day d was calculated as the evening-window mean net load minus the midday-window mean net load,

$$R_{\text{NL}}(d) = \overline{N}_{E,d} - \overline{N}_{M,d}, \tag{2}$$

where $\overline{N}_{E,d}$ and $\overline{N}_{M,d}$ are the mean net loads of day d over the evening window E = 18:00–21:00, centred on the utility's operational evening restoration period, and the midday window M = 11:00–14:00, bracketing the solar peak; both windows span $H = 3$ h.

The fast-scale tail statistic is the 99th percentile of the native 5 min absolute PV-ramp series, calculated as $|P_{\mathrm{PV}}(t) - P_{\mathrm{PV}}(t-1)|$ for daytime observations with PV output greater than 1 MW. The calculation contains n = 65,055 eligible 2025 daytime 5 min intervals. The annual extreme evening ramp R_{P99} is the 99th percentile of $R_{\mathrm{NL}}(d)$ over 314 valid 2025 daily shapes. The resource-response curves of Supplementary Section S3 use this same window pair for every resource, and each resource response $d_i(d)$ is the evening-minus-midday mean difference of that resource's output on day d. The windows were fixed ex ante before the analysis. These two metrics characterize short-timescale PV variability and daily evening net-load ramping, respectively.

Figure 1 summarizes the modelling workflow. Historical 2023–2025 records define the analysis windows and the ramp metrics of this section; quantile statistics and resource calibration supply the extreme-ramp requirement and the available response capability; the coverage margin of Section 2.3 combines the two under the scenario parameters; and the resource representation, inference, and out-of-sample protocol of Sections 2.4–2.6 qualify the planning outputs for storage, gas-fired, and hybrid options.

2.3. Scenario Construction and Coverage Margin

Scenario S modifies the measured 2025 load-side ramp and PV-drop contribution as

$$R^S(d) = R_L^{2025}(d)[1 + g_L s(\mathrm{season})] + R_{\mathrm{PVdrop}}^{2025}(d)\kappa_{\mathrm{PV}}\eta_{\mathrm{obs}}, \quad (3)$$

where $R^S(d)$ is the scenario daily evening ramp, $R_L^{2025}(d)$ and $R_{\mathrm{PVdrop}}^{2025}(d)$ are the load-shape and PV-decline components of the measured 2025 ramp on day d (the evening-minus-midday change of dispatched load and the midday-minus-evening change of PV output under the windows of Equation (2), with $R_{\mathrm{NL}}(d) = R_L(d) + R_{\mathrm{PVdrop}}(d)$), g_L is the noon-to-evening load-difference growth rate, $s(\mathrm{season})$ is the seasonal correction, specified ex ante from planning load-growth practice as 1.00 (spring), 1.25 (summer), 0.90 (autumn), and 1.15 (winter) to reflect stronger summer and winter load growth, κ_{PV} is the PV multiplier, and η_{obs} is the scenario observability correction. Scenario demand R_{P99}^S is the 99th percentile of $R^S(d)$ and uses the interpolated daily extreme-ramp composition at the planning horizon.

The five composite packages describe distinct 2030 development pathways (Table 1). S0 (2025 baseline) reproduces the measured 2025 daily shapes and resource stack. S1 (planning continuation) doubles PV output, to a peak of about 5.8 GW, with planned additions of grid-side storage, interprovincial import, and demand response (DR). S2 (PV acceleration) raises PV output 2.5-fold, to about 7.2 GW, with the S1 additions, lower PV observability, and lower import availability. S3 (resource-development lag) doubles PV output with stronger load-shape growth and no flexible-resource additions. S4 (source–grid–load–storage coordination) doubles PV output with larger storage, import, and DR additions and a longer DR duration. The PV multipliers follow the 4.61-fold growth of peak PV output over 2023–2025 with deceleration on a larger base; the load-growth rates are set conservatively relative to the observed 2023–2025 growth of the load-shape component; and the import availabilities reflect the observed decline of import response in the highest ramp bin. The battery additions of S1, S2, and S4 are grid-side, centrally dispatched storage credited through Equation (5). Distributed storage paired with self-consumption PV acts on the demand side by lowering the evening net-load ramp of Equation (3), and its growth forms a natural extension of the scenario set.

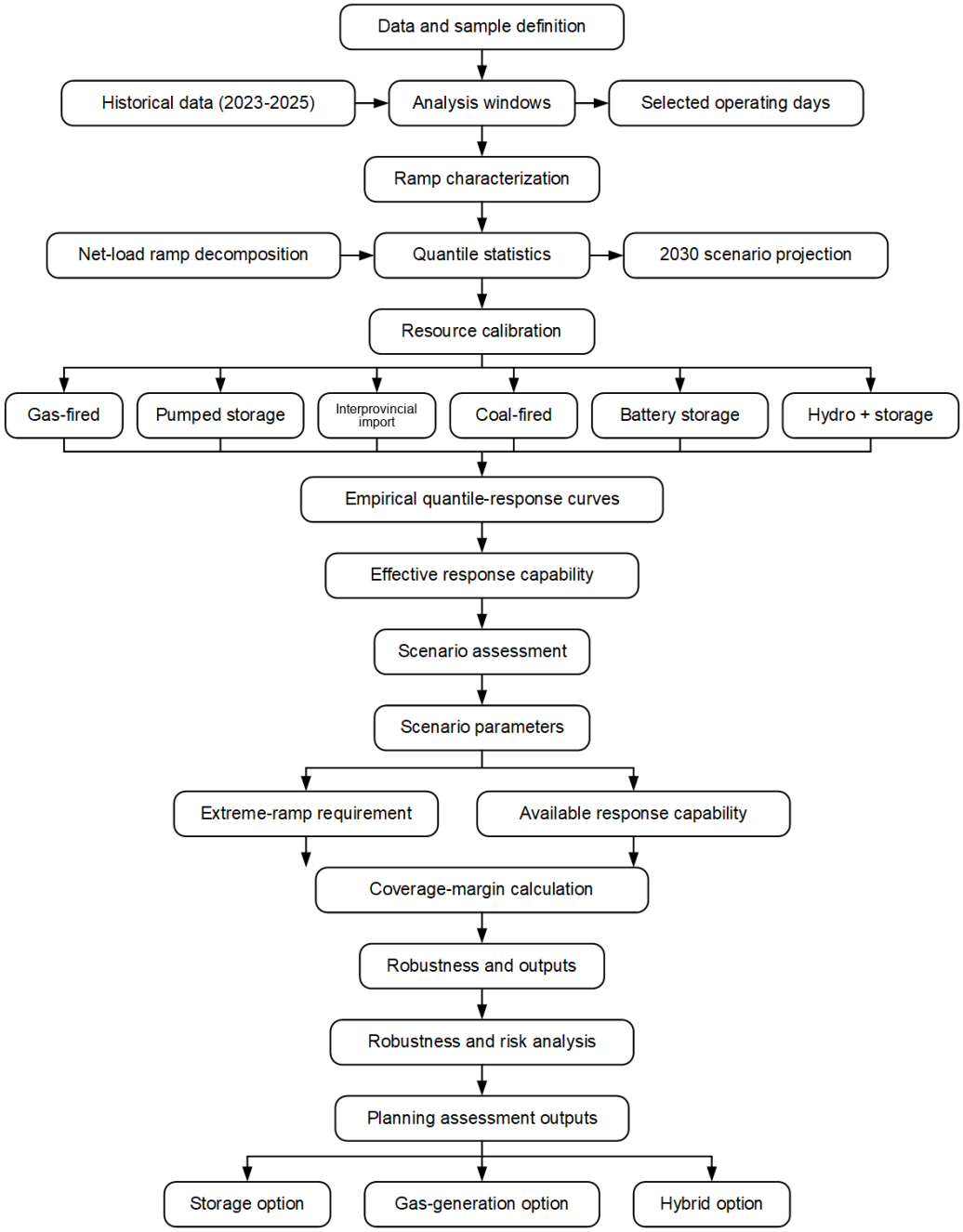


Figure 1. Integrated modelling workflow for daily extreme evening net-load-ramp planning. Historical response calibration supplies the scenario analysis, stationary block bootstrap quantifies uncertainty, and the storage-state model resolves sequential energy availability.

At normalized net-load-ramp magnitude $\rho_{\mathrm{NL}} = R_{\mathrm{P99}}/P_{\mathrm{peak}}$ and window length $H = 3$ h, the coverage margin was defined as

$$M^S(\rho_{\mathrm{NL}}, H) = \sum_i C_i^S(\rho_{\mathrm{NL}}, H) - R_{\mathrm{P99}}^S(H). \tag{4}$$

where C_i^S is the feasible contribution of resource i in scenario S, summed over gas-fired generation, coal-fired generation, interprovincial import, pumped storage, and the scenario additions of battery storage and DR, and $R_{\mathrm{P99}}^S(H)$ is the scenario extreme-ramp requirement

over the window. The feasible contribution was jointly constrained by availability, response shape, and energy capability:

$$C_i^S = a_i \min\left\{ C_i^{\text{avail}}, P_{\text{peak}}\, q_i(\rho_{\text{NL}}), \frac{E_i^{\text{avail}}}{H} \right\}. \quad (5)$$

Here, C_i^{avail} is the nameplate dispatchable capacity and E_i^{avail} is available AC-side deliverable energy. Because the response term q_i already measures a deliverable evening-minus-midday output change on the window of length H, no separate ramp-rate term enters the margin; the 5 min ramp-rate quantiles of Section S3 in the Supplementary Materials serve as variability diagnostics only. The factor a_i is the resource availability: $a_i = 1$ for every resource except interprovincial import, whose extreme-day availability $a_{\text{imp}} \in \{0.80, 0.85, 0.90\}$ multiplies the import contribution. The empirical capability curve $q_i(\rho_{\text{NL}})$ maps the normalized ramp to the deliverable response of resource i and generates the coverage margins. The curve q_i is distinct from the parametric AICc curve r_i of Table 2, which supports model selection and uncertainty analysis; the complete specification of both curve sets, the fitted parameters, and a dual-method robustness comparison of the scenario margins appear in Section S3 of the Supplementary Materials.

A negative coverage margin converts into an energy quantity through the 3 h equivalent sustainment-energy shortfall, $E_{\text{short}}^S = H \max\{0, -M^S\}$. The shortfall adopts a rectangular sustainment assumption: the uncovered power $-M^S$ is sustained across the full 3 h window, so the quantity expresses the conservative energy requirement of holding the window and upper-bounds the chronological integral of the residual power curve.

Table 1. Scenario parameters for the resource-adequacy analysis.

Scenario	κ_{PV} (–)	g_L (–)	η_{obs} (–)	a_{imp} (–)	Battery add. (MW/h)	Import add. (MW)	DR add. (MW/h)
S0 Baseline	1.0	0.00	1.00	1.00	0	0	0
S1 Continuation	2.0	0.10	0.95	0.85	1700/4	200	300/2
S2 PV acceleration	2.5	0.10	0.90	0.80	1700/4	200	300/2
S3 Resource lag	2.0	0.15	0.95	0.90	0	0	0
S4 Coordination	2.0	0.10	0.95	0.90	2200/4	500	600/3

Note: Battery and DR additions are expressed as AC-side power/duration, and battery additions are grid-side, centrally dispatched storage; deliverable energy equals power times duration (e.g., 1700 MW/4 h = 6800 MWh). The five cases are composite scenario packages.

Table 2. Resource-response curves and applicable capability quantities.

Resource	Curve	AICc Weight (–)	Response Coefficient (–)	q_i at P99 (MW)	5 min ramp P99 (MW)
Coal-fired	Linear	0.88	0.103 [0.085–0.120]	470	84.8
Gas-fired	Piecewise	0.78	0.406 [0.194–0.500]	2040	210.9
Interprovincial import	Quadratic	0.82	0.647 [0.363–0.993]	739	–
Pumped storage	Linear	0.74	0.009 [−0.043–0.065]	960	489.5

Note: The response coefficient is the fitted slope of r_i (% of peak load per % of peak load), and bracketed values are fitted intervals. The fifth and sixth columns report the empirical-curve value q_i at the 2025 annual extreme ramp and the 99th percentile of the 5 min output change; both are observed extreme-day responses, not nameplate capacities. Physical ceilings apply separately: gas saturates at the 2050 MW observed extreme-day envelope beyond the observed range and pumped storage at the 960 MW sustainable evening ceiling ($E_{\max} = 10{,}800$ MWh). Curves were fitted on 305 of 314 coverage days; bin compositions and ramp-rate quantiles appear in Section S3.

2.4. Resource-Response Curves and Pumped-Storage Representation

The parametric response curve $r_i(\rho_{\text{NL}})$ was selected by corrected Akaike information criterion (AICc) among linear, piecewise-linear, quadratic, and Hill functional forms. Table 2 reports the selected curve, AICc weight, fitted coefficient, available capacity, and associated

fast-scale ramp quantity. The resource-curve fits use 305 of the 314 coverage days. These parametric curves support model selection and uncertainty analysis; the coverage margins of Equation (5) use the empirical capability curves q_i, and Section S3 of the Supplementary Materials reports both sets together with a dual-method robustness comparison.

Pumped storage was capped at 960 MW, corresponding to 40% of the 2400 MW installed capacity; the cap represents the sustainable evening discharge ceiling observed for the station under reservoir and unit-commitment conditions, and it anchors the deliverable capability in Equation (5). The usable reservoir energy is $E_{\max} = 10{,}800$ MWh. The pumping and generating efficiencies are $\eta_c = \eta_d = 0.866$, giving a round-trip efficiency of approximately 0.75; a 3 h discharge at the 960 MW ceiling, therefore, withdraws $960 \times 3/0.866 \approx 3326$ MWh from the state. The energy-state representation was

$$E_{t+\Delta t} = E_t + \eta_c P_{c,t} \Delta t - \frac{P_{d,t} \Delta t}{\eta_d}, \qquad \mathrm{SOC}_t = \frac{E_t}{E_{\max}}. \tag{6}$$

where E_t (MWh) is the stored hydraulic energy at time t, $P_{c,t}$ and $P_{d,t}$ (MW) are the pumping and generating powers, and Δt (h) is the time step. The replenishment ratio η_r denotes the fraction of one full-power evening discharge replenished per day; $\eta_r = 1.0$ defines the full trajectory and $\eta_r = 0.3$ the constrained trajectory, under which daily replenishment equals 0.3×3326 MWh of stored hydraulic energy. A head-based 50% SOC de-rating threshold was used for stress-test sensitivity: below the threshold, deliverable pumped output scales linearly as $P_{\text{pumped}} = 960 \times \mathrm{SOC}/50\%$ MW.

Pre-coverage denotes a perfect-forecast operational upper bound: precise modeling of the evening PV decline lets dispatch pre-position slow units ahead of the evening window, so a share x% of the scenario extreme-ramp PV-decline component (3568 MW, the PV-decline component at the interpolated scenario extreme-ramp position after recombination under Equation (3)) transfers out of the evening requirement. A 10% pre-coverage share, therefore, relieves approximately 357 MW of evening demand, while the physical ramp magnitude remains unchanged.

2.5. Inference, Tail Estimation, and Analysis Samples

Uncertainty for time-dependent quantities was estimated using a stationary block bootstrap with expected block length $L = 6$ days following the Politis–Romano procedure [29]. Unless stated otherwise, the analysis used 2000 resamples (Table 3). The 95% confidence intervals for the annual extreme evening ramp and the fast-scale statistic were 4082–4511 MW and 95.9–101.4 MW, respectively. A generalized Pareto distribution fitted above the P95 threshold characterizes the cross-scale tail shape of the PV-ramp series. The quantile spectrum, block-length sensitivity, deletion tests, and cross-scale GPD diagnostics are reported in Section S2 and Figures S1 and S2 of the Supplementary Materials.

Scenario uncertainty was evaluated with a nested bootstrap–Monte Carlo procedure comprising 2000 outer stationary block resamples and triangular perturbations of the PV multiplier (±10%), g_L (±0.05, equivalent to ±5 percentage points), η_{obs} (±5%), import capability (±8%), added power (±15%), and added duration (±15%). Propagation outputs and copula-dependence results are reported in Section S4 of the Supplementary Materials.

2.6. Directional Out-of-Sample Protocol

The directional out-of-sample protocol fitted resource-response curves and the generalized Pareto model using 2023–2024 observations, then applied the locked specification to the PV-visibility-adjusted 2025 ramp input. Held-out 2025 net-load ramps and gas responses provided the comparison series. The protocol evaluates resource response conditional on PV input and tests cross-year stability within the City A dataset; external validation, which

applies the locked framework to a second city or utility system, forms the complementary validation level.

Table 3. Analysis samples and uncertainty procedures.

Analysis	Sample (Days; 5 min Intervals)	Inference or Resampling Procedure
Shapley analysis, 2023–2025	$n = 920$	200-day bootstrap
Fixed-effects variance	$n = 920$	—
Fixed-effects association	$n = 920$	5000 permutations
Quantile regression	$n = 920$	2000-day bootstrap
Resource-response curves	$n = 305$	200-day bootstrap
Fast-scale PV-ramp tail	$n = 65{,}055$; 651 exceedances	2000 blocks; $L = 6$ d
Annual extreme evening ramp	$n = 314$; ≈3 tail obs.	2000 blocks; $L = 6$ d

3. Results and Discussion

3.1. Historical Evening-Ramp Change and the Planning-Tail Target

Peak PV output increased 4.61-fold, from 625.65 MW in 2023 to 1691.40 MW in 2024 and 2885.41 MW in 2025, while the PV share of local generation rose from 2.06% to 4.12% and 8.76%; annual load growth over the same period ranged from 1.56% to 5.92%. Over this interval, the annual extreme daily evening net-load ramp increased from 2610 MW in 2023 to 3811 MW in 2024 and 4328 MW in 2025. The 2025 annual value, derived from 314 valid daily shapes, represents 18.07% of peak load and serves as the scenario baseline. The spring diagnostic was higher at 4517.56 MW (approximately 4518 MW; 18.87% of peak load; $n = 92$), and serves as a seasonal diagnostic, while the annual distribution supplies the scenario baseline (Figure 2).

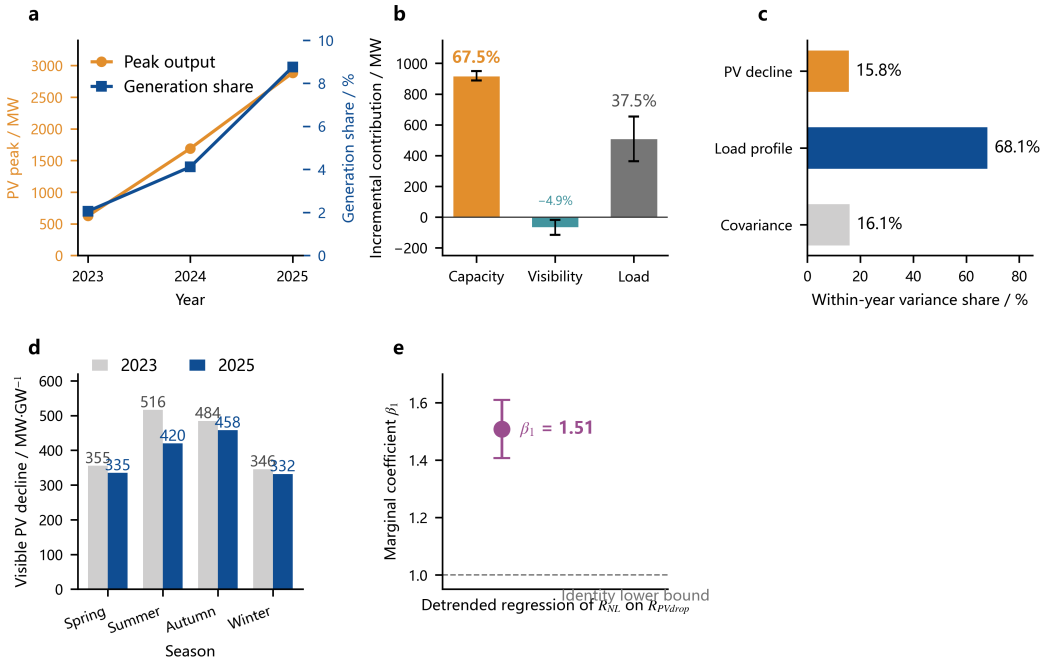


Figure 2. PV expansion and attribution of evening net-load-ramp change. The panels report annual PV output and share, the Shapley allocation of the 2023–2025 mean-ramp increment, the within-year variance decomposition, visible PV-decline intensity, and the fixed-effects association between the PV-decline and net-load-ramp components.

The fast-scale absolute PV-ramp tail and the annual extreme evening ramp describe different temporal scales. The 99th percentile of the native 5 min absolute PV-ramp series was 98.6 MW (95% CI: 95.9–101.4 MW; $n = 65{,}055$ valid 2025 daytime intervals with

PV output above 1 MW), whereas the daily-shape metric captures the aggregate evening transition. The block-bootstrap interval for the annual extreme evening ramp was 4082–4511 MW using a six-day block length. Removing the largest daily-ramp observation reduced the annual estimate to 4247 MW, and removing the three highest-ramp observations reduced it to 4202 MW. The annual planning tail, therefore, remains anchored in a cluster of high-ramp days.

The annual planning tail sits on a steep upper section of the 2025 daily distribution (Figure 3a). The type-7 interpolation places the 99th percentile between the 310th and 311th order statistics, and at that position the load-shape component contributes 2621 MW (60.57%) and the PV-decline component 1706 MW (39.43%) (Figure 3b). PV decline, therefore, supplies about two-fifths of the planning requirement in a system where PV supplies 8.76% of local generation.

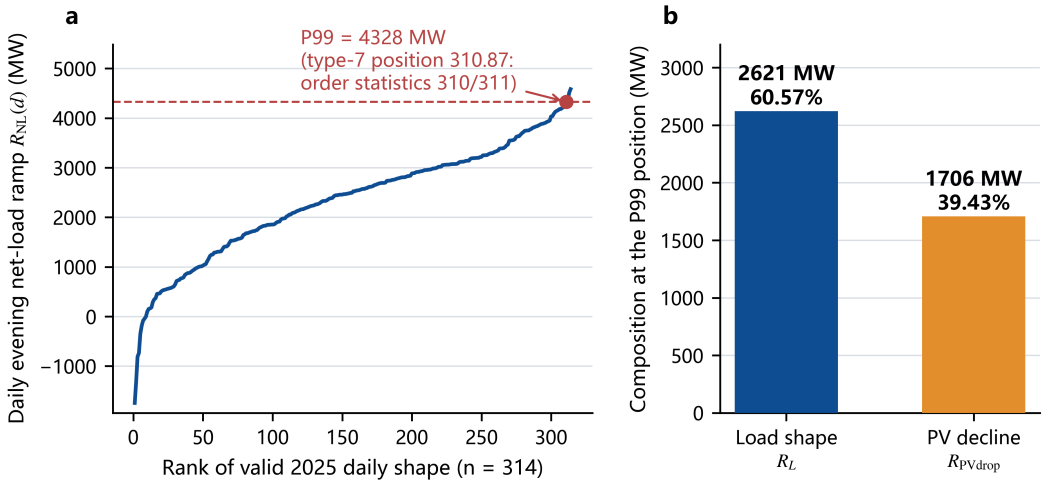


Figure 3. Annual 99th percentile of the daily evening net-load ramp in 2025. (**a**) Sorted valid daily ramps $R_{NL}(d)$ with the type-7 interpolation position of the 99th percentile (4328 MW); (**b**) composition of the interpolated 99th percentile into the load-shape component R_L and the PV-decline component R_{PVdrop}.

The ten highest evening ramps of 2025 concentrate in spring (Table 4). Eight of the ten days fall in March and April, with one winter day (12 January) and one autumn day (6 November); their ramps range from 4158 to 4583 MW (17.4–19.1% of peak load), the PV-decline component supplies 31–45% of each ramp, and daily PV peaks reach 1544–2166 MW. The ranked daily profiles of Figure 4 show the mechanism. On the highest-ramp days the midday net load forms a trough below the morning level and the evening window rises 4.2–4.6 GW above the midday mean, whereas lower-ranked days carry a smaller evening rise and their deepest deviation in the early-morning hours. Strong spring irradiance with moderate cooling load deepens the midday trough, while the evening residential and lighting load recovers fully.

The fixed-effects coefficient was 1.51 (95% CI: 1.41–1.61; $p < 0.001$; 5000 permutations; $n = 920$), with 1.0 as the mechanical-identity reference. The coefficient captures a profile-conditioned association between PV decline and the evening net-load ramp. The specified 2030 scenarios project the annual extreme evening-ramp demand to 6170–6793 MW, 25.77–28.37% of peak load and 42.56–56.95% above the 2025 baseline. These scenario ramps extend beyond the observed range of the resource-response curves (the highest observed gas-response bin sits at 17.6% of peak load), and the scenario capability, therefore, adopts a conservative convention in which the gas response saturates at its observed extreme-day envelope and holds that plateau beyond the observed range (Section S3 of the Supplementary Materials). The Shapley allocation of the 1361.6 MW mean-ramp increment assigned 918.7 MW (67.5%)

to installed capacity, −67.3 MW (−4.9%) to visibility, and 510.2 MW (37.5%) to the load profile. Together, these observational results locate the historical increase in both capacity expansion and changing daily profiles.

Table 4. The ten highest daily evening net-load ramps of 2025 and the observed evening-minus-midday resource responses.

Rank	Date	Season	R_L (MW)	R_{PVdrop} (MW)	R_{NL} (MW)	R_{NL} (% Peak)	PV Peak (MW)	Gas-Fired (MW)	Import (MW)	Pumped (MW)	Coal-Fired (MW)
1	19 Mar	Spring	2912	1672	4583	19.1	2100	2890	150	1003	487
2	20 Mar	Spring	2821	1690	4511	18.8	2081	2234	861	1239	281
3	1 Apr	Spring	2705	1653	4358	18.2	1926	2011	894	675	358
4	14 Apr	Spring	2576	1763	4339	18.1	2031	1970	853	1133	374
5	16 Mar	Spring	2928	1323	4251	17.8	1925	538	2258	1119	605
6	12 Jan	Winter	2902	1317	4219	17.6	1544	3044	−143	837	425
7	23 Mar	Spring	2568	1636	4204	17.6	1933	1287	1578	624	195
8	6 Nov	Autumn	2550	1632	4182	17.5	1916	877	1829	1254	347
9	15 Apr	Spring	2319	1862	4181	17.5	2166	2435	330	1342	202
10	2 Apr	Spring	2678	1480	4158	17.4	1939	2848	−52	575	395

Note: Resource columns report the evening-minus-midday responses $d_i(d)$ of gas-fired generation, interprovincial import, pumped storage, and coal-fired generation. The 2025 peak load of 23,944 MW normalizes the percentage column.

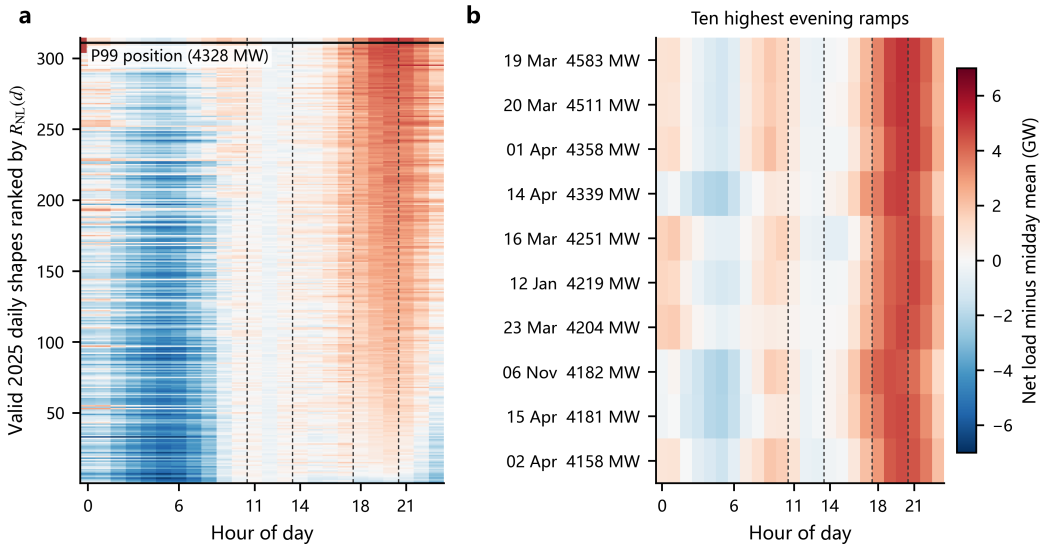


Figure 4. Ranked daily net-load profiles of 2025. (**a**) Hourly net load minus the midday-window (11:00–14:00) mean for the 314 valid daily shapes, ranked by the daily evening net-load ramp; dashed lines mark the midday and evening (18:00–21:00) windows and the solid line the 99th-percentile position. (**b**) The ten highest-ramp days of Table 4, labelled with date and $R_{\mathrm{NL}}(d)$.

3.2. Joint Resource Coverage at the Validated 2025 Target

With the planning tail established, the 2025 resource configuration provided 4212 MW of available response against an annual extreme evening-ramp requirement of 4328 MW, leaving a coverage margin of −116 MW, or −0.48% of peak load. The negative sign means that deliverable evening response falls 116 MW short of the P99 evening ramp: the 2025 portfolio covers 97.3% of the requirement, and the uncovered 116 MW held over the 3 h window corresponds to the 348 MWh equivalent sustainment-energy shortfall of Table 5. The deliverable 4212 MW lies inside the 4082–4511 MW bootstrap interval of the requirement, which places the 2025 portfolio at the coverage boundary, where a modest change in resource availability or ramp severity switches the sign of the margin. This margin is a model quantity under the historical-response capability convention: the power-balance identity makes the sum of realized resource responses track the ramp requirement by construction, and the margin departs from that identity only through the binding

physical caps, the import availability derating, and planned additions (Section S3.2 of the Supplementary Materials). Figure 5 combines conditional resource-response curves with the physical caps that determine available evening support. Over the pooled 2023–2025 daily sample ($n = 1045$, normalized by each year's corresponding peak load), the observed gas contribution rose from 1.11% of peak load in the bottom-half ramp bin to 8.76% in the top-percentile bin, while pumped storage, gas-fired generation, and interprovincial import supplied 91.7% and 94.1% of positive response in summer and winter, respectively. The single-day responses of Table 4 show how the portfolio closes individual high ramps: gas-fired generation and interprovincial import substitute for each other from day to day (on 16 March import supplied 2258 MW and gas 538 MW; on 12 January gas supplied 3044 MW while import fell by 143 MW), and pumped storage contributed 575–1342 MW.

Table 5. Annual extreme evening-ramp demand and coverage margin under the specified 2030 scenarios. The shortfall column reports the 3 h equivalent sustainment-energy shortfall $H \max\{0, -M^S\}$ under the rectangular sustainment assumption, a conservative upper bound on the chronological unserved energy.

Scenario	Demand (MW)	Response (MW)	Margin (MW)	Sust.-Energy Shortfall (MWh)	P05–P95 (MW)	Def. Prob. (%)	State
S0	4328	4212	−116	348	—	—	Near boundary
S1	6170	6029	−141	423	−528–+408	61.2	Near boundary
S2	6793	5958	−835	2505	−1256–−237	99.4	Shortfall
S3	6251	3968	−2283	6849	−2680–−1840	100.0	Shortfall
S4	6170	7225	+1055	0	+617–+1622	0.0	Positive margin

Note: Intervals and deficit probabilities arise from the nested bootstrap–Monte Carlo propagation under the gas-plateau capability (gas credited at most 2050 MW, the observed extreme-day envelope; scenario ramps exceed the observed range). The parametric curve set yields higher margins (Table S10); the S1/S2 classifications are representation-dependent, while S0, S3, and S4 classify identically under both sets.

The 2023–2024 calibration reproduced the direction of the 2025 shortfall after its parameters were locked. The held-out comparison predicted a −128 MW extreme-ramp coverage margin against the observed −116 MW value; the P95 surplus was reproduced within 5%, and the predicted ramp share of 17.85% fell within the 2025 bootstrap interval of 17.05–18.84% (4082–4511 MW). This held-out agreement establishes the cross-year stability of the calibrated response representation within the City A dataset, under its conditional-on-PV-input scope. External validation, which applies the locked framework to a second city or utility system, forms the complementary level and extends beyond the present dataset.

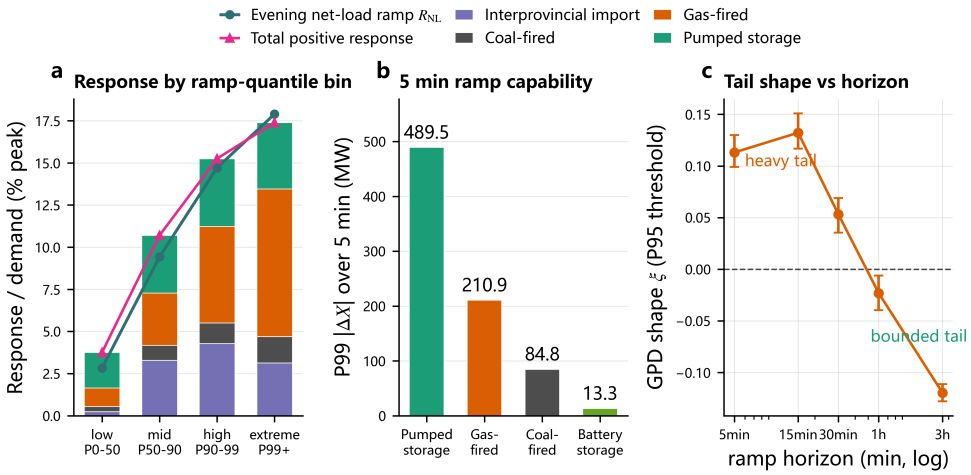


Figure 5. Quantile-dependent resource response and tail scaling. Resource contributions and 5 min capability are shown against the daily extreme evening-ramp planning target.

3.3. Scenario-Package Margins and Range-Dependent Sensitivity

With the 2025 response representation calibrated, the 2030 scenario packages span a wide range of coverage conditions (Table 5). Under the conservative observed-range capability convention, in which the gas response saturates at 2050 MW beyond the highest observed ramp bin, S1 pairs a 6170 MW requirement with 6029 MW of available response, producing a −141 MW margin; S2 pairs 6793 MW with 5958 MW, producing −835 MW. S3 combines 6251 MW of demand with 3968 MW of response, leaving a −2283 MW margin and a 6849 MWh 3 h equivalent sustainment-energy shortfall. The S3 response falls below the 2025 level of 4212 MW because S3 adds no flexible resources while the import response declines along the tail of its capability curve, from 739 MW at the 2025 extreme ramp to 276 MW at the S3 ramp; gas-fired generation and pumped storage remain at their 2050 and 960 MW ceilings. S4 reaches a +1055 MW margin from 7225 MW of available response against a 6170 MW requirement.

The nested uncertainty propagation preserves the ordering of these packages. S1, S2, S3, and S4 have P05–P95 margin ranges of −528 to +408 MW, −1256 to −237 MW, −2680 to −1840 MW, and +617 to +1622 MW, respectively; the corresponding deficit probabilities are 61.2, 99.4, 100, and 0%. The 3338 MW difference between S3 and S4 is a scenario-package contrast comprising 3257 MW associated with resource additions and 81 MW associated with higher S3 load growth. The S1–S3 margins are representation-dependent: the parametric AICc curve set of Section S3, which extrapolates a steeper gas tail beyond the observed range, yields margins up to 2.0 GW higher (S1 +1492 MW, S2 +1214 MW, S3 −589 MW), so the surplus-or-shortfall classification of S1 and S2 follows the choice of capability convention, while S0 at the boundary, S3 in shortfall, and S4 in surplus classify identically under both conventions (Table S10 of the Supplementary Materials).

Within the stated ranges of storage, PV, demand response, observability, load growth, and import availability, storage has the largest modelled first-order Sobol contribution at 0.775 (95% CI: 0.653–0.896), followed by PV at 0.160. Demand response contributes 0.026, while observability, load growth, and import availability each contribute 0.009, 0.009, and 0.008; the first-order indices sum to 0.99 and the storage total-order index is 0.787. Equal ±20% ranges reverse the leading comparison, with PV at 0.43 and storage at 0.33. The reversal arises because the first set of ranges spans staged storage additions, whereas the equal-range exercise expands the relative swing in the PV demand driver. The sensitivity ranking, therefore, follows the planning envelope. One-at-a-time perturbations and critical PV multipliers under fixed daily shapes are reported in Section S5 of the Supplementary Materials. A shortfall-valuation scan prices the 3 h equivalent sustainment-energy shortfall at 50–500 CNY/MWh: the S3 exposure rises from 0.34 to 3.42 million CNY per extreme evening, while the S0 near-boundary exposure stays below 0.18 million CNY (Figure 6d).

3.4. Duration, Sequencing, and Consecutive-High-Ramp Stress

The S3 shortfall admits several single-day closure pathways. All-storage and all-gas portfolios of 2600 MW, and a hybrid portfolio of 1560 MW storage plus 1040 MW gas, each raise available response to 6568 MW and yield an approximately +317 MW margin (Figure 7a). Their static power equivalence masks the different ways in which storage duration and gas start-up shape delivery over longer operating sequences.

With single-day closure established, the multi-period analysis separates the portfolios. Shorter-duration storage closes the single-day margin but loses availability as its energy-rate limit binds over the window, whereas the gas pathway sustains delivery across consecutive days; four-hour storage, six-hour storage, and the gas pathway each close the modelled single-day deficit. These complementary constraints motivate hybrid portfolios when both prompt delivery and sustained delivery are required.

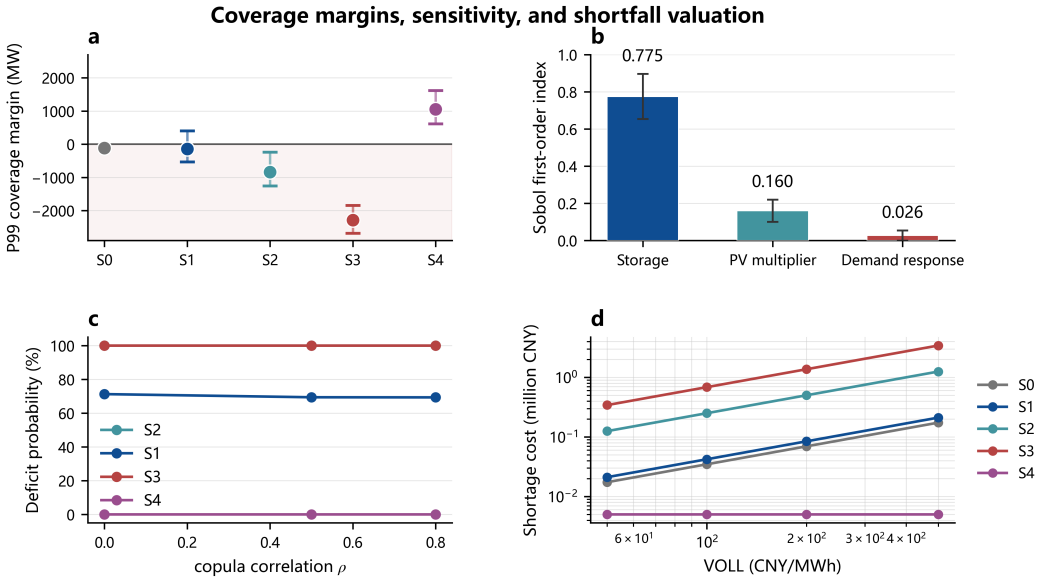


Figure 6. Coverage-margin outcomes and range-dependent sensitivity. (**a**) Deterministic scenario margins with nested bootstrap–Monte Carlo P05–P95 intervals; (**b**) Sobol first-order indices describing modelled variance contributions within the stated ranges; (**c**) deficit probability against the PV-visibility copula correlation; (**d**) valuation of the 3 h equivalent sustainment-energy shortfall, $3\,\mathrm{h} \times (-M^S) \times \mathrm{VOLL}$, over a VOLL scan of 50–500 CNY/MWh.

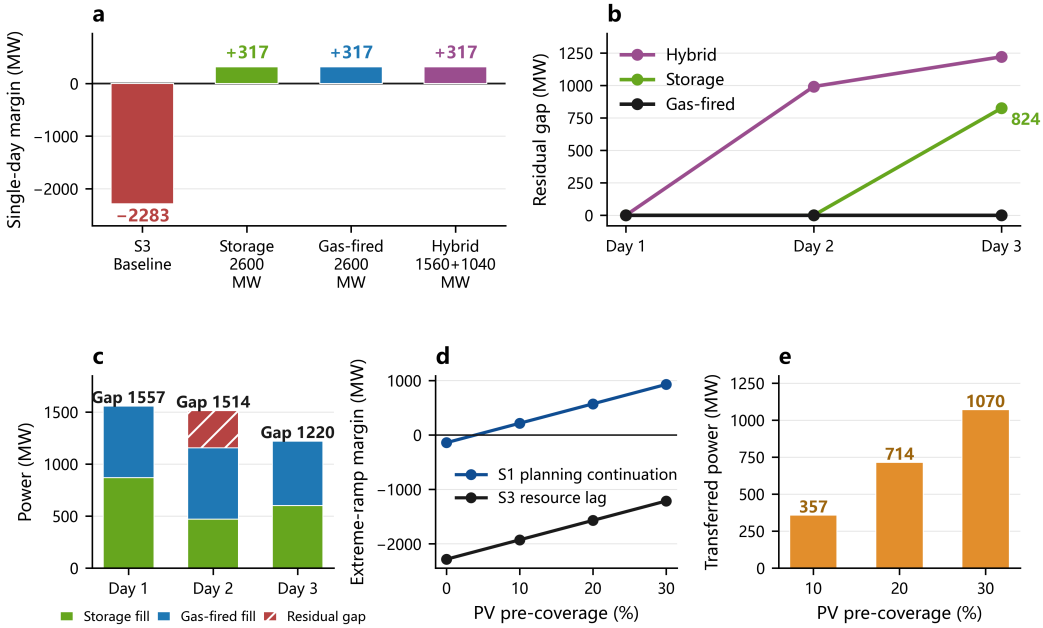


Figure 7. Static deficit-closure pathways and upper-bound pre-coverage sensitivity. (**a**) Single-day margins for the S3 baseline and the three 2600 MW closure pathways; (**b**) residual evening gap over three consecutive high-ramp days per pathway; (**c**) storage fill, gas-fired fill, and residual gap for the observed 19–21 March episode; (**d**) coverage margins against the PV pre-coverage share; (**e**) PV-decline component transferred ahead of the window. Equal single-day power margins carry different duration and sequencing properties.

The March and April 2025 high-ramp sequences expose the intertemporal limit of static closure (Figure 8a). For 19–21 March, the upper-bound daily residual series was 1557, 1514, and 1220 MW, with a 3 h equivalent cumulative residual energy of 1.29×10^4 MWh under the same rectangular sustainment assumption as the sustainment-energy shortfall. With $\eta_r = 0.3$, SOC declined from 100% to 78.4%, 56.9%, and 35.3% across days one to three (Figure 8b). On days four and five, SOC fell to 22.8% and 18.0%, pumped-storage output

declined from 960 MW to 678 MW and 438 MW, and the residual rose from 1220 MW to 1502 MW and 1743 MW. The stress sequence, therefore, shifts the binding condition from single-day power capacity to recoverable energy. The full observed–extrapolated SOC trajectories, threshold sensitivity, and validation matrix are reported in Sections S6 and S7 of the Supplementary Materials.

Perfect-forecast pre-coverage provides an upper-bound operational comparison (Figure 7d,e). Each additional 10-percentage-point pre-coverage share transfers approximately 357 MW of the scenario extreme-ramp PV-decline component out of the evening window; at 10%, the S1 margin increases from −141 to +216 MW, while the S3 margin increases from −2283 to −1926 MW and reaches −1213 MW at 30%. These results are consistent with the multi-day stress case: scheduling reduces the critical-window burden, and replenishable flexible-resource capacity sustains coverage across consecutive days.

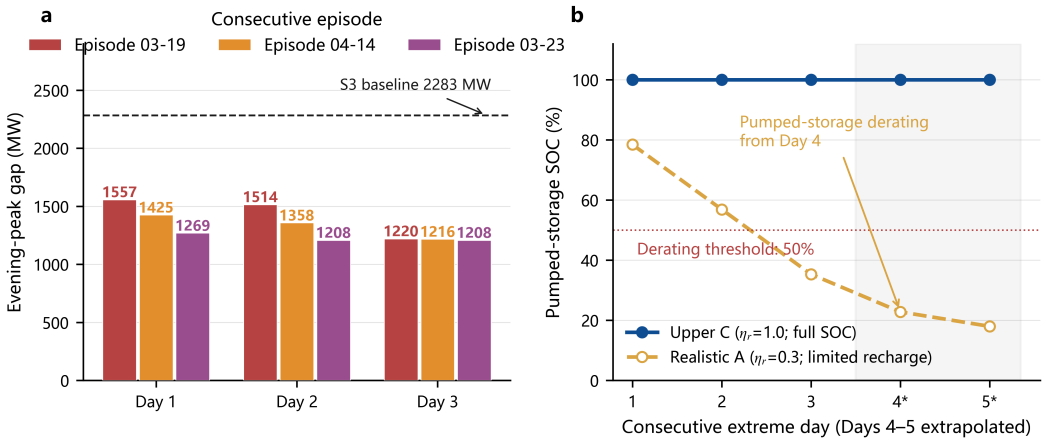


Figure 8. Consecutive high-ramp stress and pumped-storage state. (**a**) Observed daily evening gaps for the episodes starting 19 March, 14 April, and 23 March 2025; the dashed line marks the S3 single-day deficit. (**b**) SOC trajectories for the 19–21 March episode under full and constrained replenishment; days 4* and 5* are stress-test extrapolations under the stated replenishment and threshold assumptions, not observations.

4. Conclusions

This study shows that adequacy for evening balancing pressure is determined by whether deliverable resource capability, spanning power output, sustained energy, and interday replenishment, covers the annual extreme evening net-load ramp, and by what margin. In City A, that requirement rose from 2610 MW in 2023 to 4328 MW in 2025 (18.07% of peak load) as peak PV output grew 4.61-fold.

The 2025 portfolio operates with little slack: it delivers 4212 MW against the 4328 MW requirement and sits at its coverage boundary (−116 MW, −0.48% of peak load) under the historical-response capability convention, and the 2030 outlook amplifies this narrow margin toward either a persistent shortfall (−2283 MW under resource-development lag, deficit probability 100%) or a comfortable surplus (+1055 MW under coordinated development, 0%) depending on how quickly and coherently source, grid, load, and storage resources are developed. The held-out stability check, which predicts −128 MW against the observed −116 MW, supports the transferability of the calibrated response curves across years within the City A dataset and within their conditional-on-PV-input scope; under the historical-response capability convention, the narrow margin reflects a persistent property of the current portfolio across calibration samples.

These results recast flexible-resource planning as the coordinated configuration of power, deliverable energy per window, storage duration, and recoverable energy. Portfolios with equal single-day power margins of +317 MW diverge over consecutive high-ramp

days, because storage duration and interday replenishment determine whether coverage persists: under constrained replenishment, pumped-storage SOC falls from 100% to 35.3% within three days of the 19–21 March episode. Advance pre-positioning shifts part of the critical window, about 357 MW per 10% pre-coverage share, and replenishable capability sustains coverage beyond that shift. The framework transfers to other receiving-end cities after local recalibration of solar profiles, load shapes, interprovincial import conditions, and storage inventories.

The findings carry direct implications for grid operation and electricity markets. In operation, the extreme-ramp margin identifies the clear-sky spring days on which slow units are pre-positioned day ahead, pumped-storage SOC is managed across consecutive high-ramp days, and evening import schedules are protected. In markets, the margin provides a quantity basis for ramping products sized to the evening transition [16–18] and for capacity remuneration that differentiates storage duration [15], and the valuation scan places the resource-lag exposure at 0.34–3.42 million CNY per extreme evening.

The reported margins serve as planning comparisons across the scenario pathways examined here. Resource capability is calibrated on historically observed maximum responses. The validation operates at two levels: the held-out check establishes cross-year stability within the City A dataset, and external validation, which tests the calibrated curves against data from another city, would extend the generality of the coverage-margin approach. Extending the planning horizon across multiple years, jointly optimizing storage power and energy capacity, and incorporating stochastic replenishment together with investment costs are the next steps toward least-cost portfolio screening alongside coverage-margin assessment.

Supplementary Materials: The following supporting information can be downloaded at https://www.mdpi.com/article/10.3390/en19235769/s1, Section S1 (data sources and quality audit), Section S2 (tail statistics and stability), Section S3 (resource-response constraints), Section S4 (scenario propagation), Section S5 (single-day boundary), Section S6 (consecutive-day SOC trajectories), Section S7 (sensitivity, validation, and city transfer), including Tables S1–S15 and Figures S1–S6.

Author Contributions: Conceptualization, Y.G., J.L. and H.L.; methodology, Y.G. and J.L.; validation, H.D. and F.Z.; formal analysis, Y.G. and J.L.; investigation, H.D. and F.Z.; data curation, Y.G. and J.L.; writing—original draft preparation, Y.G. and J.L.; writing—review and editing, H.D., F.Z. and H.L.; visualization, Y.G. and J.L.; supervision, H.L.; project administration, H.L.; funding acquisition, H.L. All authors have read and agreed to the published version of the manuscript.

Funding: This research was funded by the Guangdong Power Grid Co., Ltd./Guangzhou Power Supply Bureau Grid Planning Special Project, grant number 030100QQ00250004.

Institutional Review Board Statement: Not applicable.

Informed Consent Statement: Not applicable.

Data Availability Statement: The data presented in this study are not publicly available because they originate from restricted utility operational records and are subject to confidentiality and data-governance requirements.

Acknowledgments: The authors acknowledge Guangzhou Power Supply Bureau for providing access to the operational records used in this study.

Conflicts of Interest: Authors Yanna Gao, Hong Dong and Fanhong Zeng were employed by the company Guangzhou Power Supply Bureau, Guangdong Power Grid Co., Ltd. The remaining authors declare that the research was conducted in the absence of any commercial or financial relationships that could be construed as a potential conflict of interest.

References

1. National Energy Administration. 2025 Photovoltaic Power Generation Construction Status. Available online: https://www.nea.gov.cn/20260305/4216fa1274bd4b7f8da92090ba3999aa/c.html (accessed on 8 November 2026). (In Chinese)
2. North American Electric Reliability Corporation. *Distributed Energy Resources: Connection Modeling and Reliability Considerations*; NERC: Atlanta, GA, USA, 2017.
3. International Energy Agency. *Unlocking the Potential of Distributed Energy Resources*; IEA: Paris, France, 2022. https://doi.org/10.1787/a2ed7a25-en.
4. Zhang, J.; Liu, H.; Wang, Y.; Zhu, Y.; Yuan, J. Effect of flexible ultra-high-voltage power transmission on receiving power systems in China. *Energy Rep.* **2023**, *9*, 70–79. https://doi.org/10.1016/j.egyr.2023.04.322.
5. Liu, Y.; Jiang, Z.; Guo, B. Assessing China's provincial electricity spot market pilot operations: Lessons from Guangdong province. *Energy Policy* **2022**, *164*, 112917. https://doi.org/10.1016/j.enpol.2022.112917.
6. He, Y.; Liu, Y.; Li, M.; Zhang, Y. Benefit evaluation and mechanism design of pumped storage plants under the background of power market reform—A case study of China. *Renew. Energy* **2022**, *191*, 796–806. https://doi.org/10.1016/j.renene.2022.03.070.
7. Hou, Q.; Zhang, N.; Du, E.; Miao, M.; Peng, F.; Kang, C. Probabilistic duck curve in high PV penetration power system: Concept, modeling, and empirical analysis in China. *Appl. Energy* **2019**, *242*, 205–215. https://doi.org/10.1016/j.apenergy.2019.03.067.
8. Lannoye, E.; Flynn, D.; O'Malley, M. Evaluation of power system flexibility. *IEEE Trans. Power Syst.* **2012**, *27*, 922–931. https://doi.org/10.1109/TPWRS.2011.2177280.
9. Lannoye, E.; Flynn, D.; O'Malley, M. Transmission, variable generation, and power system flexibility. *IEEE Trans. Power Syst.* **2015**, *30*, 57–66. https://doi.org/10.1109/TPWRS.2014.2321793.
10. Heggarty, T.; Bourmaud, J.Y.; Girard, R.; Kariniotakis, G. Quantifying power system flexibility provision. *Appl. Energy* **2020**, *279*, 115852. https://doi.org/10.1016/j.apenergy.2020.115852.
11. Kato, T. Public data-driven modeling of residual electricity load due to high penetration of photovoltaic power generation in various distribution networks. *IFAC-Pap.* **2023**, *56*, 390–395. https://doi.org/10.1016/j.ifacol.2023.10.1599.
12. Jia, X.; Zhang, J.; Pan, N.; Yang, J.; Xiao, R. Net load forecasting for high renewable penetration grids: Hybrid decomposition and multi-scale temporal convolutional network. *Int. J. Electr. Power Energy Syst.* **2026**, *176*, 111686. https://doi.org/10.1016/j.ijepes.2026.111686.
13. Ulbig, A.; Andersson, G. Analyzing operational flexibility of electric power systems. *Int. J. Electr. Power Energy Syst.* **2015**, *72*, 155–164. https://doi.org/10.1016/j.ijepes.2015.02.028.
14. You, L.; Ma, H.; Saha, T.K. A CVaR-constrained optimal power flow model for wind integrated power systems considering transmission-side flexibility. *Int. J. Electr. Power Energy Syst.* **2023**, *150*, 109087. https://doi.org/10.1016/j.ijepes.2023.109087.
15. Li, C.; Jiang, Y.; Dai, J.; Guo, R. Capacity market in the decarbonization era: Adequacy, flexibility, and environmental revenue. *IET Renew. Power Gener.* **2024**, *18*, 3944–3954. https://doi.org/10.1049/rpg2.13084.
16. Wang, B.; Hobbs, B.F. A flexible ramping product: Can it help real-time dispatch markets approach the stochastic dispatch ideal? *Electr. Power Syst. Res.* **2014**, *109*, 128–140. https://doi.org/10.1016/j.epsr.2013.12.009.
17. Sreekumar, S.; Yamujala, S.; Sharma, K.; Bhakar, R.; Simon, S.P.; Rana, A.S. Flexible ramp products: A solution to enhance power system flexibility. *Renew. Sustain. Energy Rev.* **2022**, *162*, 112429. https://doi.org/10.1016/j.rser.2022.112429.
18. Ghaljehei, M.; Khorsand, M. Day-ahead operational scheduling with enhanced flexible ramping product: Design and analysis. *IEEE Trans. Power Syst.* **2022**, *37*, 1842–1856. https://doi.org/10.1109/TPWRS.2021.3110712.
19. Blakers, A.; Stocks, M.; Lu, B.; Cheng, C. A review of pumped hydro energy storage. *Prog. Energy* **2021**, *3*, 022003. https://doi.org/10.1088/2516-1083/abeb5b.
20. Javed, M.S.; Ma, T.; Jurasz, J.; Amin, M.Y. Solar and wind power generation systems with pumped hydro storage: Review and future perspectives. *Renew. Energy* **2020**, *148*, 176–192. https://doi.org/10.1016/j.renene.2019.11.157.
21. Huertas-Hernando, D.; Farahmand, H.; Holttinen, H.; Kiviluoma, J.; Rinne, E.; Söder, L.; Milligan, M.; Ibáñez, E.; Martín-Martínez, S.; Gómez-Lázaro, E.; et al. Hydro power flexibility for power systems with variable renewable energy sources: An IEA Task 25 collaboration. *WIREs Energy Environ.* **2017**, *6*, e220. https://doi.org/10.1002/wene.220.
22. Sepulveda, N.A.; Jenkins, J.D.; Edington, A.; Mallapragada, D.S.; Lester, R.K. The design space for long-duration energy storage in decarbonized power systems. *Nat. Energy* **2021**, *6*, 506–516. https://doi.org/10.1038/s41560-021-00796-8.
23. Dowling, J.A.; Rinaldi, K.Z.; Ruggles, T.H.; Davis, S.J.; Yuan, M.; Tong, F.; Lewis, N.S.; Caldeira, K. Role of long-duration energy storage in variable renewable electricity systems. *Joule* **2020**, *4*, 1907–1928. https://doi.org/10.1016/j.joule.2020.07.007.
24. Denholm, P.; Hand, M. Grid flexibility and storage required to achieve very high penetration of variable renewable electricity. *Energy Policy* **2011**, *39*, 1817–1830. https://doi.org/10.1016/j.enpol.2011.01.019.
25. Mallapragada, D.; Sepulveda, N.; Jenkins, J. Long-run system value of battery energy storage in future grids with increasing wind and solar generation. *Appl. Energy* **2020**, *275*, 115390. https://doi.org/10.1016/j.apenergy.2020.115390.
26. Dratsas, P.A.; Psarros, G.N.; Papathanassiou, S.A. Contribution of PV generation with embedded battery storage to capacity adequacy. *IEEE Trans. Sustain. Energy* **2025**, *16*, 1125–1138. https://doi.org/10.1109/TSTE.2024.3505413.

27. Tan, Q.; Wang, Y.; Wen, X.; Qiao, L. Cross-regional peak-shaving scheduling for the hybrid pumped storage–wind–photovoltaic complementary system. *Energy* **2025**, *326*, 136119. https://doi.org/10.1016/j.energy.2025.136119.
28. Xiao, Y.; Ye, H.; Ge, Y.; Huang, Y.; Wang, H. Coordinated planning of flexibility resources for HVDC-connected renewable base and load center: A CVaR-based probabilistic approach. *IET Renew. Power Gener.* **2026**, *20*, e70193. https://doi.org/10.1049/rpg2.70193.
29. Politis, D.N.; Romano, J.P. The stationary bootstrap. *J. Am. Stat. Assoc.* **1994**, *89*, 1303–1313. https://doi.org/10.1080/01621459.1994.10476870.

Disclaimer/Publisher's Note: The statements, opinions and data contained in all publications are solely those of the individual author(s) and contributor(s) and not of MDPI and/or the editor(s). MDPI and/or the editor(s) disclaim responsibility for any injury to people or property resulting from any ideas, methods, instructions or products referred to in the content.